Fisher Information and the Combination of RGB Channels

Reiner Lenz* and Vasileios Zografos

Department of Science and Technology and Department of Electrical Engineering, Linköping University, SE-601 74 Norrköping, Sweden
reiner.lenz@liu.se
Department of Electrical Engineering, Linköping University, SE-581 83 Linköping, Sweden
zografos@isy.liu.se

Abstract. We introduce a method to combine the color channels of an image to a scalar valued image. Linear combinations of the RGB channels are constructed using the Fisher-Trace-Information (FTI), defined as the trace of the Fisher information matrix of the Weibull distribution, as a cost function. The FTI characterizes the local geometry of the Weibull manifold independent of the parametrization of the distribution. We show that minimizing the FTI leads to contrast enhanced images, suitable for segmentation processes. The Riemann structure of the manifold of Weibull distributions is used to design optimization methods for finding optimal weight RGB vectors. Using a threshold procedure we find good solutions even for images with limited content variation. Experiments show how the method adapts to images with widely varying visual content. Using these image dependent de-colorizations one can obtain substantially improved segmentation results compared to a mapping with pre-defined coefficients.

Keywords: Fisher information, Weibull distribution, information geometry, RGB2Gray mapping.

1 Introduction

Combining the information from several color channels into one scalar value is one of the basic operations in color processing [1–3]. A typical example is the separation of the color information into a scalar-valued intensity and a vector-valued chromaticity component. Often the mapping is constructed such that the resulting image takes into account the properties of human observers. Another popular choice is to preserve certain characteristics of the color image, such as gradient information, as far as possible in the scalar image.

* This work was supported by the Swedish Foundation for Strategic Research through grant IIS11-0081 and the European Community's Seventh Framework Programme FP7/2007-2013 - Challenge 2 - Cognitive Systems, Interaction, Robotics - under grant agreement No 247947 - GARNICS.

S. Tominaga, R. Schettini, and A. Trémeau (Eds.): CCIW 2013, LNCS 7786, pp. 250–264, 2013.

In this paper we use methods from information geometry to explore different mappings based only on statistical properties of the image. We make no assumptions about the purpose of the conversion or the nature of the input images. We only assume that the raw sensor data has undergone some basic processing (in our example edge detection). We use the Fisher information framework (for applications in different scientific fields see [4]) and introduce the Fisher-Trace-Information (FTI) as the trace of the Fisher information matrix. The FTI depends only on the geometry of the Weibull manifold and we will show that minimizing the FTI leads to scalar images with good contrast which are also suitable inputs to automatic segmentation procedures.

The processing steps are the following: We filter the R, G and B components of the image separately with L filter functions resulting in the images $R_1, G_1, B_1, \ldots R_L, G_L, B_L$. For a given weight vector $x = \left(x_R, x_G, x_B\right)$ we combine the filter images obtaining $F_l = x_R R_l + x_G G_l + x_B B_l$. In the last step the strength of the filter result in each pixel p, denoted by $Y(p) = \|F_1(p), ..., F_L(p)\|$ is computed. As a result we have a set of non-negative values y, one for every point in the image. We assume that they follow a parametrized probability distribution $W(y;\theta)$. The theory of information geometry shows how to provide the set of probability distributions with the structure of a Riemann manifold where the local geometry is described by the Fisher matrix. For the parameter θ, estimated from the data, we define the value of the cost function $C(\theta)$ as a function of the Fisher information matrix at $W(y;\theta)$. Compared to approaches based on covariances, this has the advantage that the value of the cost function will only depend on the intrinsic geometrical properties of the manifold but not on the coordinate system used to describe the measurements. Since θ depends on the weight vector x we also write $C(x)$ instead of $C(\theta)$. Finally we select the optimal weight vector $\widehat{x}$ such that $C(\widehat{x})$ has a minimum value and generate the scalar image as the linear combination $\widehat{x}_R R + \widehat{x}_G G + \widehat{x}_B B$.

The experiments show that the mapping takes into account the statistical properties of the RGB image and lead to gray-value images with higher contrast than those obtained by a weight vector with fixed coefficients. We also show how the manifold structure of the Weibull distributions can be used in optimization methods to estimate optimal weight vectors for a given image. The details of this construction and some implementation issues will be described in Sec. 2. Experiments illustrating some results obtained can be found in Sec. 3.

2 Theoretical Background and Implementation

In the previous section we introduced the non-negative magnitude values $Y(p)$ as descriptors of the visual content at pixel position p. We also assume that those points p in the image where the value $Y(p)$ differs significantly from its average are visually most important. Here we consider only the case where the important points are those with high magnitude values. We are therefore interested in the probability distribution of the largest values. From probability theory it is

known that the limit distribution of properly normalized maxima of a sequence of independent and identically distributed random variables is given by the generalized extreme value distribution. This distribution is therefore often used to model the maxima of long sequences of random variables. This motivates the application of the Weibull distribution, which is a special type of the generalized extreme value distribution, to describe the statistical properties of the selected magnitude values (see also [5–8]). Here we choose to describe the statistical distributions of the filter results by the 2-parameter Weibull distribution. We use the notation and the results in [9] and define the (2-parameter) Weibull distribution by its cumulative density function (CDF) as

$$W(y;\lambda,\beta) = 1 - exp(-(y/\beta)^{\lambda}) \tag{1}$$

where λ is the shape and β is the scale parameter. It is defined for positive values of y. There is also a 3-parameter version with an extra degree of freedom (location parameter), which gives the flexibility of fitting to a larger range of filtered images [10, 11]. The drawback is that the geometry of the 3-parameter Weibull is more complicated and therefore we often fit a 3-parameter Weibull, extract the location parameter and then subtract it from the data, effectively removing that extra degree of freedom. The location is often of little interest and as a result we have a 2-parameter Weibull, with the same properties (scale and shape parameters) as the original distribution. The estimation of the location parameter is computationally expensive and when execution time is important we replace it with the minimum value of the samples.

The Weibull distributions defined in Eq.(1) depend on two parameters and information geometry (see [12, 13]) shows how to equip this space of Weibull distributions with a Riemannian geometry, in which properties such as distances, angles and geodesics may be defined. The 2-parameter Weibull manifold looks locally like a plane and the geometry is defined by a metric on the tangent space at each point. This metric is given by the symmetric, positive-definite Fisher matrix G with three elements $g_{ij}(\theta) = \int \frac{\partial \log p(x,\theta)}{\partial \theta_i} \frac{\partial \log p(x,\theta)}{\partial \theta_j} p(x,\theta) dx$ where x is the stochastic variable and θ is the parameter vector. For the two-parameter Weibull distribution given by the shape-scale pair (λ,β) we have $\theta = (\lambda,\beta)$ and the matrix elements of the Fisher matrix are given as (see [9] and [14]):

$$g_{11} = \frac{\lambda^2}{\beta^2}; \qquad g_{12} = \frac{\gamma - 1}{\beta}; \qquad g_{22} = \frac{1 - 2\gamma + \gamma^2 + \pi^2/6}{\lambda^2}, \tag{2}$$

where $\gamma \approx 0.577216$ is Euler's constant.

As a symmetric 2×2 matrix the Fisher matrix G is completely defined by the determinant, the trace and the angle of the first eigenvector. Both the determinant and the trace are parameters that are independent of the parametrization of the manifold depending only on the local geometrical properties of the manifold. We use the trace and refer to it as the Fisher-Trace-Information (FTI). We select the minimum of the FTI as our cost function and the experiments will show that this choice leads to gray-value images with good contrast which

are also suitable as input for segmentation procedures. The FTI defines the cost function C:

$$C(\lambda, \beta) = \mathrm{tr}(g_{ij}) = g_{11} + g_{22} = \frac{6 + 6(\gamma - 2)\gamma + \pi^2 + 6\lambda^4/\beta^2}{6\lambda^2}. \tag{3}$$

A contour plot of the trace is shown in Fig. 1 which illustrates the relation between the parameters of the distribution and the cost function.

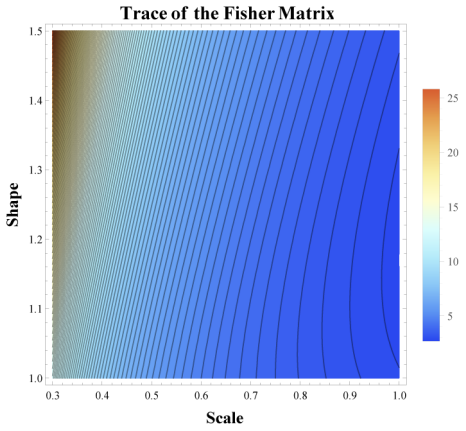

Fig. 1. Weibull distribution: trace as function of (scale,shape) parameters

A major advantage of the fact that the Weibull distributions form a 2D manifold is the possibility to compute derivatives. In applications two vector fields are of importance: one that is defined through the cost function C and one that describes the changes related to a change of parameters. For the cost function we get the (negative) gradient field

$$dC = \left(-\frac{\partial C}{\partial \lambda}, -\frac{\partial C}{\partial \beta}\right) = \left(\frac{2\left(-1+(2-\gamma)\gamma-\pi^2/6+\lambda^4/\beta^2\right)}{\lambda^3}, -2\lambda^2/\beta^3\right) \tag{4}$$

For a path p given by weight vectors $p(t) = \big(\rho(t), \gamma(t), 1 - \rho(t) - \gamma(t)\big)$ we can compute the vector field

$$dP = \left(\frac{\partial \lambda}{\partial t}, \frac{\partial \beta}{\partial t}\right) \tag{5}$$

Assuming euclidean geometry we can use the chain-rule and combine them as

$$\frac{dC}{dt} = -\frac{\partial C}{\partial \lambda}\frac{\partial \lambda}{\partial t} - \frac{\partial C}{\partial \beta}\frac{\partial \beta}{\partial t} \tag{6}$$

or, in the manifold framework, we can use the Fisher matrix $G(\lambda, \beta)$ with the elements defined in Eq. 2, as a metric which results in:

$$\left(-\frac{\partial C}{\partial \lambda} \; -\frac{\partial C}{\partial \beta}\right) G(\lambda, \beta) \begin{pmatrix} \frac{\partial \lambda}{\partial t} \\ \frac{\partial \beta}{\partial t} \end{pmatrix} \tag{7}$$

Standard optimization methods can then be used to find the weight vector with the smallest trace value that minimizes the cost function.

In all our experiments we use the dihedral, edge-type filters on a 5×5 window. These filters are constructed using the representation theory of the dihedral group which is the symmetry group of the grid with quadratic pixels. Application of these filters is similar to the FFT with the only difference that the group of the discrete shift operators is replaced by the dihedral group D(4). From the general theory it follows that there are six filter pairs that transform like common edge-detection filters $(e_x^{(1)}, e_y^{(1)}, \ldots, e_x^{(6)}, e_y^{(6)})$. In the notation of the previous section we thus have $L = 12$. These filters are applied for each of the R, G and B-channels separately and they only need to be computed once for a given RGB-image. Following the description in the previous section we have to apply the weight vector and introduce a magnitude or length value for the result. In our experiments we used two different variations of this construction. In the first construction we first compute the linear combinations of the R,G and B-filter results from one filter (say filter number l) to obtain the filter results $g_x^{(l)}, g_y^{(l)}$. The magnitude value is then calculated as the sum of the norms of vectors with the filter pairs $y = \sum_l \|(g_x^{(l)}, g_y^{(l)})\|$. This requires the availability of all 12 x 3 filter result images during the optimization process. We avoid this in the second algorithm where we combine the raw filter results first for each band and then we combine these results using the weight vectors. If $y_R = \sum_l \|(e_x^{(l)}, e_y^{(l)})\|$ is the result for the red channel and y_g, y_B the corresponding magnitude results for the green and blue band then the final magnitude value is computed as linear combination $x_R y_R + x_G y_G + x_B y_B$. This requires only that the three magnitude filter images are available during the optimization. In general both methods lead to similar results and we usually use the 3-magnitude filter version in our experiments. A detailed description of the dihedral filters can be found in [15–17] but other choices of edge-detectors, or other derivative-type filters, such as Gabor filters can also be used.

We mentioned above that we often fit a 3-parameter Weibull first, extract the location parameter and then subtract it from the data. This first step is computationally expensive when the location parameter is estimated with the help of a maximum-likelihood fitting method. We therefore often replace the location parameter with the minimum value. This gives slightly inferior but acceptable results. In optimization experiments where the Weibull parameters have to be estimated several times we often use this faster, minimum-based estimation method to obtain better start values for the more accurate location-based computation.

For images with very limited visual variations we introduce a threshold process in which only the points with the highest edge magnitudes are included in the fitting. Using such a threshold has several advantages: practically it speeds up computation since only a fraction of the original data has to be processed and it implements the intuitive requirement that points with low edge magnitude values are visually less important. Finally we mention that we use an R^2 goodness of

fit test [18] to measure the goodness of fit of the Weibull distributions to the data samples.

3 Experiments

In Fig. 2 we illustrate the constructions introduced in the previous section with the help of a typical RGB-image. In this experiment we vary the parameter vector along the line $(t, 1/3, 2/3 - t), 0 \leq t \leq 2/3$. The blue arrows in the plot show the (negative) gradient vectors dC defined in Eq. 4. They describe the change of the trace of the Fisher matrix as a function of the scale and shape parameters. The red arrows are samples of the vector field dP defined in Eq. 5 as the weight vector varies along the line $(t, 1/3, 2/3 - t)$. The scalar image at the beginning of the curve (with the highest trace value, located in the upper left corner of the vector plot) and the scalar image with the lowest value of the trace are (located in the lower right corner of the plot), together with the original color image, are shown in the middle- and the right side of Figure 3. We see that the resulting images clearly separate into areas with different dominating colors whereas the fixed-coefficient conversion used by rgb2gray maps all objects to relatively similar gray values.

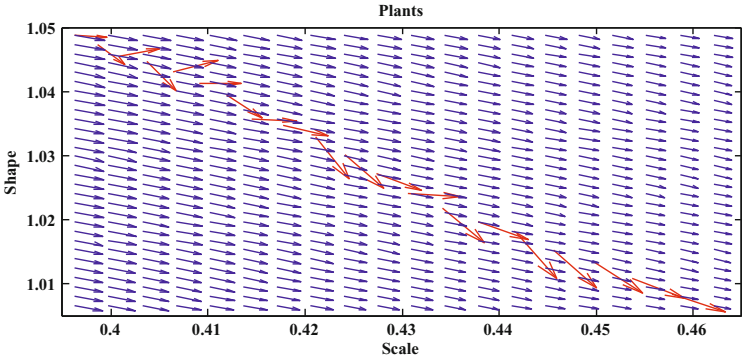

Fig. 2. Vector field for variations along the red/blue line and the trace gradients

Fig. 3. Original image, highest/lowest trace value (red/blue variation)

In Figs. 4,5a and 5b we illustrate the effect of the threshold used to suppress points with low magnitude filter values. In these experiments we used 50%, 20% and 5% of the pixels with the highest filter values (i.e. quantile values $q = 0.5, 0.8, 0.95$). We then fitted a Weibull distribution to the remaining points and finally we evaluate the goodness of the fit with the help of the R^2-test. In these figures the image in the upper left corner is the original color image, the other three images (labeled (I), (II) and (III) in the figures) show the results for different threshold settings arranged in increasing R^2-values. The image (labeled as (III)) in the lower right corner has the highest R^2-value indicating the best fit. The numerical values for the R^2 measure and the corresponding threshold levels are collected in Table 1 and the images obtained are shown in Figs. 4 and 5. We see that in these examples the threshold values that resulted in the highest R^2 values also produced the best gray value image with a better discrimination between the different color regions.

Table 1. R^2 goodness of fit values for different threshold values

	Fig.4			Fig.5a			Fig.5b		
label	(I)	(II)	(III)	(I)	(II)	(III)	(I)	(II)	(III)
q	0.95	0.5	0.8	0.5	0.8	0.95	0.95	0.5	0.8
R^2	0.81	0.89	0.89	0.924	0.945	0.98	0.951	0.959	0.973

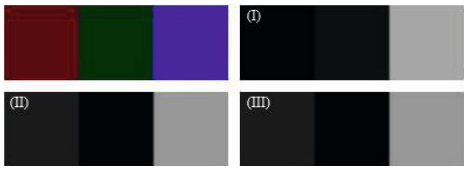

Fig. 4. Homogeneous squares

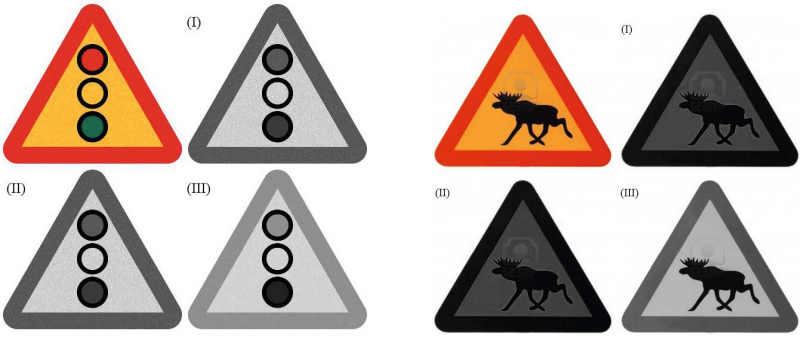

(a) Trafic Sign 1 (b) Trafic Sign 2

Fig. 5. Mapping of traffic signs

Depending on the image content the path on the Weibull space can be much more complicated than the situation illustrated in Fig. 2. This is illustrated in Figs. 6,7 and 8. Fig. 6 corresponds to Fig. 2 showing the vector fields defined by the trace and the parameter change. Fig. 7 shows 16 of the images generated by varying the weight vectors along the line $(t, 1/3, 2/3-t), 0 \leq t \leq 2/3$. The variation of the trace values along the parameter curves $(1/3, t, 2/3-t), (t, 1/3, 2/3-t), (t, 2/3-t, 1/3)$ is shown in Fig. 8. The trace values for the images in Fig.7 are those that follow the black solid curve in Fig. 8. Comparing this curve and the images in Fig. 7 confirms the motivation behind the cost function is valid since it shows that a low trace value (at the beginning and the end of the curve) corresponds indeed to images with richer visual content.

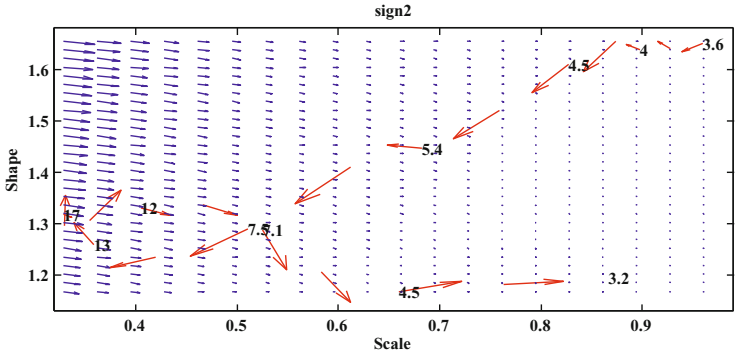

Fig. 6. Traffic Sign variation

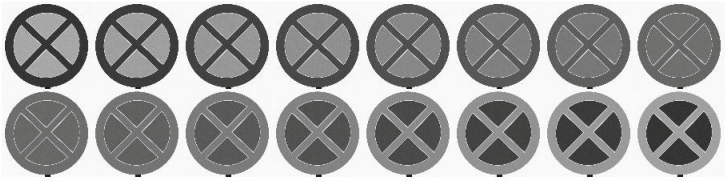

Fig. 7. Traffic Sign variations; parameter interval $(t, 1/3, 2/3-t), 0 \leq t \leq 2/3$

In Eqs. 6 and 7 we described how the geometric structure of the Weibull manifold can be used to compute changes of the cost function. We used this in a simple implementation of an optimization method based on a line-search along a color coordinate axis. We implemented it as follows: first we define a coordinate

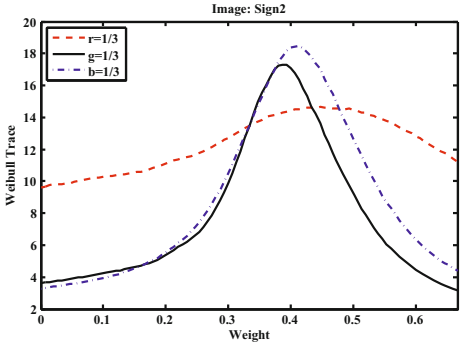

Fig. 8. Trace values for parameter variations along the coordinate axes

direction in RGB space by fixing one of the color components and varying the RGB vectors along the remaining two colors. For a given starting point we find first the direction with the highest initial decrease of the cost function and then start a line-search along that direction until we find a minimum point. The new point is then used as starting point in the next line-search iteration along another color component. An illustration of the results obtained by such an optimization is shown in Figs. 9a and 10. The change of the RGB weight vectors during one such optimization (together with the corresponding trace values) is shown in Fig. 9b. The number of search directions was limited to eight in this case. Compared with Matlabs rgb2gray mapping one can see that the optimization generated a similar image but with a slightly higher contrast. This is a general property we observed in our experiments: When the color image has a rich variation of colors then the optimization methods results usually in weight vectors that are very similar to standard fixed vectors. When the color distribution in the original image is more extreme, for example consisting mainly of red/blue pixels, then the optimized weight vectors is very different and better adapted to the properties of the original. In the experiments described here we use Eq. 6 in the optimization. We compared results from both, Eqs. 6 and 7 and found that they almost always agree on the direction of the descent, what differs is the length of the vectors which might be useful when more advanced optimization methods are used.

In the beginning we mentioned that we used two different ways incorporating a third parameter into the Weibull fitting. In one approach we subtract the location parameter of the three-parameter Weibull distribution before fitting a two-parameter Weibull distribution. In the other method we subtract the minimum value instead. The images in Fig 11 show that for some images the Weibull-location solution leads to visibly different results with lower trace values. Fig. 11a shows the original image, Fig. 11b the result of the optimization incorporating the minimum subtraction and Fig. 11c starts with the weight

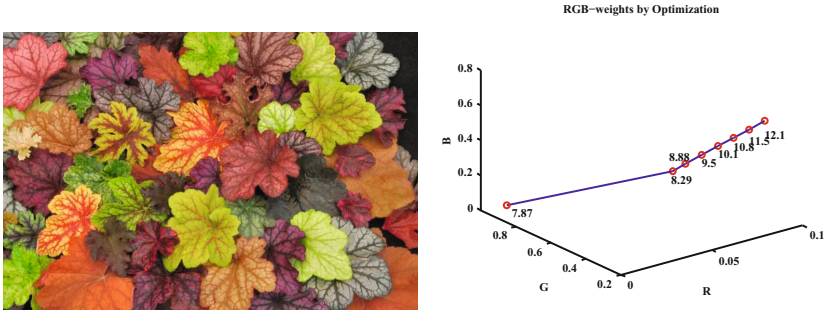

(a) Original (b) RGB vectors

Fig. 9. Colorful image

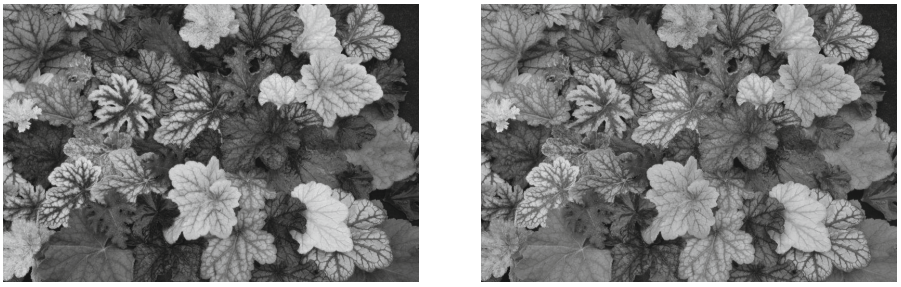

(a) Result of optimization (b) Matlab rgb2gray

Fig. 10. Optimized mapping compared to Matlabs RGB2Gray

vector found in the minimum-based method and applies an additional optimization step making use of the Weibull-location parameter. For comparison we show the result of applying the RGB2Gray function provided by Matlab.

Our proposed mapping is not designed to optimize visual similarity to aid human observers but instead it attempts to increase the separation of the different channels in the resulting grayscale image. This can be considered as a type of contrast enhancement. As a result the Fisher-based mapping is well suited as input to segmentation methods. We will illustrate this property with a superpixel segmentation experiment on the two images in Fig 11c(c) and (d).

A superpixel is a perceptually meaningful collection of pixels, obtained from some low-level grouping process. Given this definition, the elements (pixels) inside each superpixel form a consistent unit, e.g. in terms of color, texture, intensity and so on. In this particular example we will use the relaxation labeling superpixel method by [19], which works on grayscale intensity. In other words, each superpixel is defined by the mean and variance of its constituent pixels' intensities and it is adapting its shape towards strong intensity boundaries. This is exactly the kind of information our proposed mapping enhances.

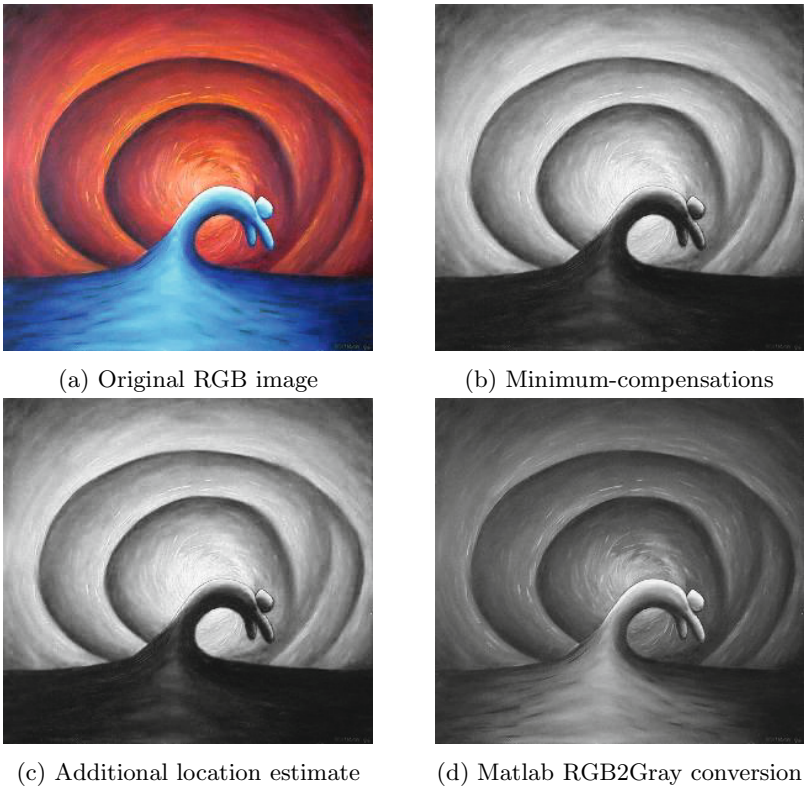

(a) Original RGB image (b) Minimum-compensations

(c) Additional location estimate (d) Matlab RGB2Gray conversion

Fig. 11. The effect of minimum and location subtraction

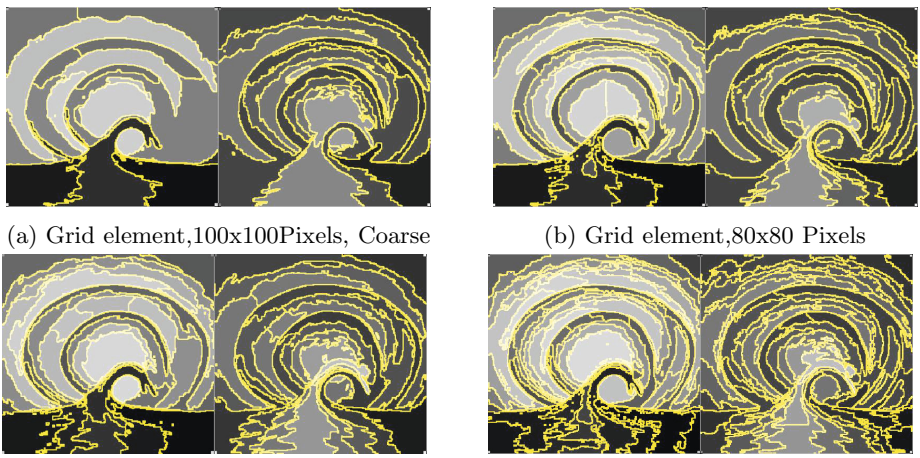

(a) Grid element,100x100Pixels, Coarse (b) Grid element,80x80 Pixels

(c) Grid element,60x60 Pixels (d) Grid-element,40x40 Pixels,Fine

Fig. 12. Superpixel segmentation results of intensity mapped images (left Fisher trace optimization, right Matlab rgb2gray) at different levels of detail

The first stage to superpixel segmentation is initialization by a randomly labeled square grid. The size of the grid (granularity) determines the level of detail of the superpixel segmentation but also its speed. At coarser scales the segmentation is very fast but a lot of the details are lost especially along weak boundaries. It is obvious that we need a good mapping that will optimize the trade off between speed and level of detail.

In Fig. 12 we see the superpixel segmentation applied to the mapping result images from Fig 11c(c) and (d) at different grid levels. At the finer levels Fig. 12(d) both images produce similar boundaries (overlaid). However, as we increase the coarseness the two segmentation results diverge. Notice how Matlab's RGB2Gray degenerates much faster (already from 60x60 pixel element grids) due

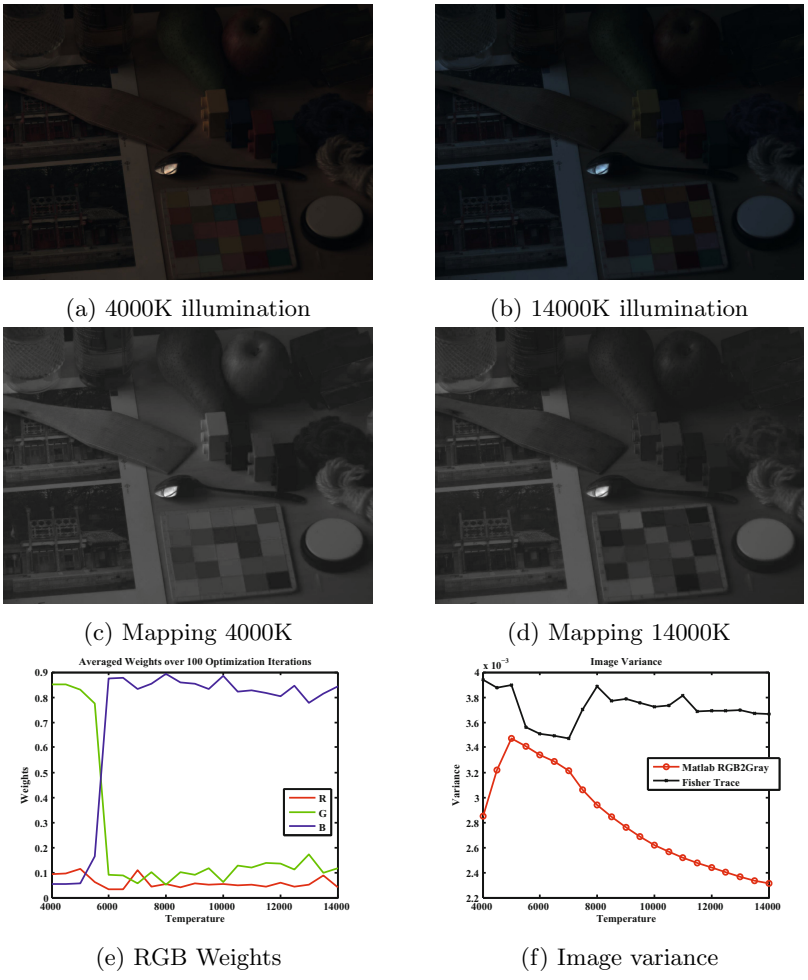

(a) 4000K illumination (b) 14000K illumination

(c) Mapping 4000K (d) Mapping 14000K

(e) RGB Weights (f) Image variance

Fig. 13. The effect illumination changes

to the weak contrast boundaries it produces. By the coarsest grid where each element has 100x100 pixels, the foreground figure has completely disappeared. The Fisher-based mapping however conserves a lot of the boundary information at much coarser levels due to the good contrast separation. As a result, we may say that this type of mapping is ideal in cases where we wish to obtain a result suitably for fast, intensity-driven segmentation.

In the last example we illustrate the effect of illumination changes. We start with a multi-spectral image with 31 channels in 10nm steps from 410nm to 710nm. We then used a mathematical model of a digital camera to simulate a (linear) raw RGB image. As illumination we selected black-body radiators with temperatures from 4000K to 14000K in 500K steps. In Fig. 13 we see the simulated raw images for the 4000K and 14000K illuminations and the optimized scalar images. The curves that show the three components of the weight vectors as a function of temperature of the illuminating radiator. These curves were obtained by averaging the results over 100 different iterations with random start points. The image variance in the scalar images for one Fisher trace mapping and the fixed rgb2gray mapping are shown in Fig. 13f.

(a) Original

(b) Trace

(c) rgb2gray

Fig. 14. Example images with pure colors

Note that the RGB images shown here are the linear RGB images without gamma mapping. The high intensity for some points on the spoon leads to a rather dark overall linear RGB image. The results obtained here, illustrate how the weights change from a red-green combination for a reddish illumination to a blue-green combination for the blueish illumination. It also shows that the image variance for the trace-based conversion is always higher than the variance in the images produced with rgb2gray. Some additional examples, using images with only pure colors and demonstrating the flexibility of the method, are shown in Fig. 14. They show that the mapping improves the separation between regions with different color properties compared to the fixed-coefficient mapping implemented in rgb2gray.

4 Summary and Conclusions

We introduced the trace of the Fisher matrix of the Weibull distribution as a cost function that defines the quality of linear combinations of the RGB channels of a color image. We also used the manifold structure of the Weibull distribution to design optimization algorithms to find the minimum points of the cost function. Our experiments show that for images with limited edge variations, such as traffic signs, it is important to limit the distribution fitting to the most significant edge pixels. We also showed that the trace measures visually significant appearance changes where low trace values correspond to higher contrast images. We also implemented different optimization algorithms and showed that they produce mappings resulting in images with better contrast and separability properties. Preliminary results show that the optimization methods produce weight vectors that adapt to changing illumination conditions.

In this paper we selected the edge-like filters in the dihedral filter system but other contrast filters, for example line-filters or any combination of them could also be used. The framework can also be used to select the filter functions and their optimal weights. The optimization used here consists of a simple line-search along coordinate axes. More efficient optimization methods along general search directions and with more advanced line-search methods can be used to improve the performance of the method. The investigation of the illumination changes are only an illustration of one experimental setup. A detailed investigation of the influence of the different parameters (such as the camera model, quantization, noise etc.) is outside the scope of this paper.

References

1. Socolinsky, D., Wolff, L.: Multispectral image visualization through first-order fusion. IEEE Trans. Image Processing 11(8), 923–931 (2002)
2. Alsam, A., Drew, M.: Fast colour2grey. In: IS&T/SID Color Imaging Conference, pp. 342–346 (2008)
3. Finlayson, G., Connah, D., Drew, M.: Lookup-table-based gradient field reconstruction. IEEE Trans Image Processing 20(10), 2827–2836 (2011)

4. Frieden, B.R., Gatenby, R.A.: Exploratory Data Analysis Using Fisher Information. Springer (2007)
5. Geusebroek, J.M., Smeulders, A.W.M.: Fragmentation in the vision of scenes. In: Proc. IEEE Int. Conf. Comp. Vision, pp. 130–135 (2003)
6. Geusebroek, J.-M.: The Stochastic Structure of Images. In: Kimmel, R., Sochen, N.A., Weickert, J. (eds.) Scale-Space 2005. LNCS, vol. 3459, pp. 327–338. Springer, Heidelberg (2005)
7. Gijsenij, A., Gevers, T.: Color constancy using natural image statistics and scene semantics. IEEE Trans. Pattern Anal. Mach. Intell. 33(4), 687–698 (2011)
8. Wichmann, F.A., Hill, N.J.: The psychometric function: I. fitting, sampling, and goodness of fit. Perception & Psychophysics 63(8), 1293–1313 (2001)
9. Oller, J.M.: Information metric for extreme value and logistic probability distributions. Sankhya: The Indian J. of Stat., Series A (1961-2002) 49(1), 17–23 (1987)
10. Zografos, V., Lenz, R.: Spatio-chromatic Image Content Descriptors and Their Analysis Using Extreme Value Theory. In: Heyden, A., Kahl, F. (eds.) SCIA 2011. LNCS, vol. 6688, pp. 579–591. Springer, Heidelberg (2011)
11. Rinne, H.: The Weibull Distribution: A Handbook. CRC Press (2008)
12. Amari, S., Nagaoka, H.: Methods of information geometry. Translations of mathematical monographs, vol. 191. American Mathematical Society (2000)
13. Murray, M., Rice, J.: Differential geometry and statistics. Monographs on Statistics and Applied Probability, vol. 48. Chapman and Hall (1993)
14. Cao, L., Sun, H., Wang, X.: The geometric structures of the Weibull distribution manifold and the generalized exponential distribution manifold. Tamkang Journal of Mathematics 39(1), 45–52 (2008)
15. Lenz, R.: Investigation of receptive fields using representations of dihedral groups. Journal of Visual Communication and Image Representation 6(3), 209–227 (1995)
16. Lenz, R., Bui, T.H., Takase, K.: A group theoretical toolbox for color image operators. In: Proc. ICIP 2005, pp. III–557–560. IEEE (2005)
17. Lenz, R., Zografos, V., Solli, M.: Dihedral Color Filtering. In: Advanced Color Image Processing and Analysis. Springer (2012)
18. Sheskin, D.: Handbook of parametric and nonparametric statistical procedures. Chapman & Hall/CRC, Boca Raton (2004)
19. Mester, R., Conrad, C., Guevara, A.: Multichannel Segmentation Using Contour Relaxation: Fast Super-Pixels and Temporal Propagation. In: Heyden, A., Kahl, F. (eds.) SCIA 2011. LNCS, vol. 6688, pp. 250–261. Springer, Heidelberg (2011)